remote sensing

MDPI

Article

SAR and ASCAT Tropical Cyclone Wind Speed Reconciliation

Weicheng Ni [1,2], Ad Stoffelen [3], Kaijun Ren [1,2,*], Xiaofeng Yang [4] and Jur Vogelzang [3]

[1] College of Meteorology and Oceanography, National University of Defense Technology, Changsha 410073, China
[2] College of Computer Science and Technology, National University of Defense Technology, Changsha 410073, China
[3] Department of Satellite Observations, Royal Netherlands Meteorological Institute, 3731 GA De Bilt, The Netherlands
[4] State Key Laboratory of Remote Sensing Science, Aerospace Information Research Institute, Chinese Academy of Sciences, Beijing 100101, China
* Correspondence: renkaijun@nudt.edu.cn

Abstract: Wind speed reconciliation across different wind sources is critically needed for extending available satellite wind records in Tropical Cyclones. The deviations between wind references of extremes, such as the moored buoy data and dropsonde wind estimates for guidance on geophysical model function development, are one of the main causes of wind speed differences for wind products, for instance, the overestimation of Synthetic Aperture Radars (SARs) relative to ASCAT winds. The study proposes a new wind speed adjustment to achieve mutual adjustment between ASCAT CMOD7 winds and simultaneous SAR wind speeds. The so-called CMOD7D-v2 adjustment is constructed based on the statistical analysis of SAR and ASCAT Tropical Cyclone acquisitions between 2016 and 2021, showing a satisfactory performance in wind speed reconciliation for winds with speeds higher than 14 m/s. Furthermore, the error characteristics of the CMOD7D-v2 adjustment for Tropical Cyclone winds are analyzed using the Triple Collocation analysis technique. The analysis results show that the proposed wind adjustment can reduce ASCAT wind errors by around 16.0% when adjusting ASCAT winds to SAR wind speeds. In particular, when downscaling SAR winds, the improvement in ASCAT wind errors can be up to 42.3%, effectively alleviating wind speed differences across wind sources. Furthermore, to avoid the impacts of large footprints by ASCAT sensors, wind speeds retrieved from SAR VV signals (acting as a substitute for ASCAT winds) are adjusted accordingly and compared against SAR dual-polarized winds and collocated Stepped Frequency Microwave Radiometer (SFMR) observations. We find that the bias values of adjusted winds are lower than products from other adjustment schemes by around 5 m/s at the most extreme values. These promising results verify the plausibility of the CMOD7D-v2 adjustment, which is conducive to SAR and ASCAT wind speed comparisons and extreme wind analysis in Tropical Cyclone cases.

Keywords: Tropical Cyclone; wind speeds; Synthetic Aperture Radar; ASCAT; wind adjustment

Citation: Ni, W.; Stoffelen, A.; Ren, K.; Yang, X.; Vogelzang, J. SAR and ASCAT Tropical Cyclone Wind Speed Reconciliation. *Remote Sens.* **2022**, *14*, 5535. https://doi.org/10.3390/rs14215535

Academic Editor: Yukiharu Hisaki

Received: 6 September 2022
Accepted: 31 October 2022
Published: 2 November 2022

1. Introduction

Tropical Cyclones (TCs) are among the most destructive natural disasters, making coastal economies vulnerable to extreme wind force, heavy rain, and dramatic storm surges. Space-borne remote sensing plays an essential role in global TC monitoring. Microwave sensors, such as scatterometers and Synthetic Aperture Radars (SARs), have the unique capability of cloud penetration and can provide all-weather ocean surface roughness (Normalized Radar Cross Section, NRCS) measurements. A series of Geophysical Model Functions (GMFs), mapping wind vectors to NRCS values measured by satellite sensors, have been developed during recent decades [1–4] to achieve accurate estimates of ocean surface winds. In particular, the CMOD7 [5] and MS1AHW [6] are the two most state-of-art GMFs for scatterometer and SAR wind vector retrieval, respectively. These wind retrieval

algorithms are usually trained with different in situ wind reference bases, mainly moored buoy or dropsonde wind measurements.

However, the concern of wind reference qualities is often ignored, which is one of the causes of wind measurement inconsistency between different wind sources. The moored buoy data are generally used as the absolute reference for scatterometer GMF calibration [7,8]. To date, many operational scatterometers and the European Centre for Medium-Range Weather Forecasts (ECMWF) follow the moored buoy scale due to their perceived accuracy. However, there is a controversy on the quality of buoy measurements in rough seas, where buoys have been thought to be impacted by sheltering caused by large waves and elevation changes, thus leading to negative biases. These concerns refer back to the research by [9,10]. However, the recent C-band High and Extreme-Force Speeds (CHEFS) project [7] (funded by the European Organization for the Exploitation of Meteorological Satellites, EUMETSAT) made a thorough investigation of the integrity of buoy winds and found that the impacts can be well-calibrated [11], addressing the concerns about the moored buoy capability for high-wind calibration and validation. As such, moored buoy data can be considered of good quality, though largely absent for the most extreme winds. The credibility of moored buoy data has been verified for extreme winds up to 25 m/s, and above 25 m/s, only sporadic data exist [7,12]. On the other hand, Stepped Frequency Microwave Radiometer (SFMR) observations, calibrated by dropsonde wind profiles [13], are the current sole available spatial wind observations for satellite-based sensors, with TC wind sensitivity up to about 75 m/s and dispersion of 5 m/s [8,13]. Nevertheless, several quality issues remain for dropsonde winds at 10 m height, as well as for the representativeness of dropsondes for SFMR winds [14]. The accuracy of the position, speed, and deceleration processing of the sonde near the surface [7,11] has not been investigated, which can result in systematic biases and hence contaminate the 10 m winds obtained. Such errors are speed-dependent, highlighting the importance of an improved assessment of the sonde processing near the surface, where the deceleration is maximum [7,15]. In addition, SFMR winds show increased variance in high winds and an evident wind speed overestimation compared to scatterometer wind estimates at extreme winds [16]. The deviations between these two wind references highlight the importance of building a more reliable and general wind reference for high and extreme winds, which will contribute to extending available satellite wind records of TCs.

In service of this goal, satellite instrument intercalibration of extremes is necessary [17], and thus calls for relevant investigations. However, it is a dilemma which kind of in situ measurements researchers should put more confidence in [11] and how to best calibrate winds to achieve wind consistency. Calibration and validation of wind estimates from multiple platforms are popular in present research, while commonly against one wind speed reference of choice. For example, several studies have attempted to calibrate satellite winds (e.g., scatterometers, altimeters, and radiometers) against moored buoy measurements for operational and longer-term climatological applications [18–20], given their proven high accuracy. Furthermore, the calibration of reanalysis data [21,22] by satellite winds is often required for large marine areas and particularly under cyclonic conditions. However, wind estimates from SAR, SFMR, and dropsonde are often excluded. On the other hand, SFMR measurements are widely used for SAR wind calibration and GMF developments [3,4,6,23] for new satellite sensors. Note that a direct comparison between dropsonde and buoy wind measurements in actual circumstances is nearly impossible because encounters are rare. As a result, the comparison is generally operated across satellite winds retrieved with different wind reference bases. Chou et al. [24] investigated the Advanced Scatterometer (ASCAT) winds (following the moored buoy wind speed scale) versus global dropsonde observations, showing a systematic negative bias at high and extreme winds. However, the bias can be effectively mitigated by a quadratic regression fit (noted as Chou-2013). Tamizi et al. [25] made an assessment for the Chou-2013 adjustment by comparing adjusted winds to TC winds approximated by the Holland model [26], exhibiting a slight underestimation for most scatterometers. On the other hand, the recent analysis by Polverari

et al. [16] shows a similar result, which is that there exists a high correlation between ASCAT CMOD7 winds and SFMR measurements at extremes; hence, the wind speed differences can be removed by an appropriate correction scheme (noted as Polverari-2021 or CMOD7D adjustment). The finding is further verified by the independent investigation by Ribal et al. [27], who developed polynomial relationships between different scatterometers and SFMR measurements.

Nevertheless, considering high wind variability in dropsonde estimates and the growing number of TC observations by SARs (generally calibrated by SFMR measurements, and hence indirectly by dropsonde estimates), a specific wind adjustment scheme for wind speed reconciliation between ASCAT and SAR winds is required before comparison. As such, in this study, a new wind speed adjustment method (named CMOD7D-v2 adjustment in the paper to be distinct from the one by Polverari et al.) taking advantage of historical SAR and ASCAT CMOD7 TC wind fields is tested. The experimental results suggest that the proposed CMOD7D-v2 adjustment can achieve a good consistency between ASCAT and SAR winds.

The experimental results illustrate that the high wind speed discrepancy between dropsonde-based SAR and buoy-based ASCAT winds at extremes can be efficiently removed using a suitable wind adjustment scheme. It contributes to building a more credible wind reference in the future and hence improves the training of GMFs. In addition, the adjusted SAR wind speeds are correlated linearly with ASCAT and ECMWF winds, which implies the potential of uncertainty and error evaluation for these three wind systems in TC conditions, taking advantage of the Triple Collocation analysis technique [28]. The obtained error variances of observation (SAR and scatterometer winds) and background (ECMWF model forecasts) will benefit the usage of 2-Dimensional variational ambiguity removal (2DVAR) for wind ambiguity removal [29–31] in TC conditions, and subsequently conducive to the observation assimilation for improving TC track and intensity forecasting [32–34]. Moreover, the adjusted SAR TC winds can act as auxiliary information and play a role in future ASCAT TC winds' spatial resolution enhancement.

2. Materials

2.1. RadarSat-2 and Sentinel-1 SAR Images

Since 2016, European Space Agency (ESA) has set up specific SAR acquisition campaigns (Satellite Hurricane Observations Campaign, SHOC) to maximize SAR acquisitions in TCs. SHOC helps to collect SAR acquisitions for both RadarSat-2 (RS-2) [35] and Sentinel-1 (S1) [36] missions and thus feeds research and development activities. RS is one of the first satellites onboarding a cross-polarized mode that is more sensitive to extreme wind speeds. It is generally considered one of the most advanced Earth observation radar image sources and has been widely used in TC research [23,37–39]. The S1 mission was a constellation of two satellites (S1-A and -1B), which orbited Earth 180° apart and offered a revisit time of around six days. End 2021 S1-B stopped functioning and will be replaced by S1-C. The high spatial resolution of SAR enables it to capture refined TC characteristics and thus provide independent measurements of TC metrics [40]. In this study, two kinds of GMFs are used to retrieve SAR winds: the MS1AHW GMF for SAR dual-polarized (VV+VH) signals and the CMOD7 GMF for SAR co-polarized (VV) signals.

2.2. ASCAT Data

ASCAT is one available scatterometer type used routinely for near-real-time TC observation, weather warnings, and forecasting. In this study, the ASCAT-A and ASCAT-B winds are processed by the ASCAT wind data processor (AWDP) [41] on a swath grid of 12.5 km. The CMOD7 GMF is used in the inversion step of the wind retrieval. The wind ambiguities are removed using the 2DVAR scheme, in which ECMWF operational forecasts are used as background winds. The observation and background error variances are left at their default 2DVAR values. Note that ECMWF surface winds need to be spatially shifted first to match the TC centres in ASCAT data. A further description of ECMWF forecast

winds is presented in Section 2.3. For the collocation between ASCAT and ECMWF winds, we refer to [41]. AWDP generally collects three ECMWF forecasts around the ASCAT acquisition time and then performs spatial and time interpolations successively (refer to [42] for interpolation details) to interpolate forecasts to ASCAT Wind Vector Cell (WVC) positions. However, TC structures move quickly and exhibit vigorous convection, resulting in artefacts and TC smearing after spatial–time interpolations. As such, only the forecast step closest to ASCAT acquisition time is used to interpolate to ASCAT WVC positions, and the time interpolation is not adopted.

2.3. ECMWF Forecasts

The ECMWF winds used in this study are short-range forecasts of 10 m stress-equivalent winds [7] generated by the ECMWF Integrated Forecasting System (IFS) model. The IFS model, which is currently operational, combines state-of-the-art meteorological and atmospheric composition modelling [43], capable of providing deterministic hourly predictions in a grid spacing of around 9 km. The research by Li et al. [44] found that the size of TC eyes generally ranges from hundreds to thousands of square kilometres. Thus, the datasets used in this study under TC conditions appear justified. A high wind speed consistency between ASCAT and ECMWF winds has been demonstrated in the CHEFS report [7].

2.4. SFMR Observations

SFMR observations are spatial wind observations directly calibrated against dropsondes in TCs. The quality of SFMR measurements has been greatly improved during recent decades [13,45,46]. Until now, SFMR measurements have become the critical data source for TC research and are widely used for model training and product validation purposes [47–49]. The SFMR datasets used in this study are provided by the NOAA Ocean Surface Winds Team (OSWT) and the U.S. Air Force Reserve Command (AFRC) for operational surface wind measurements. Though noisy, they have been calibrated using the WL150 algorithm [13]. Note that low-quality SFMR data are filtered out based on the quality flag included. The data collocation between SFMR observations and SAR images is performed following the criterion of maximizing the correlation coefficients between SFMR wind speeds and SAR VH measurements in each SFMR flight leg in order to match the TC centres in SFMR and SAR, cf. [37].

3. Methods

Aiming to explore the exact wind speed retrieval differences between ASCAT and SAR wind products at extremes, RS-2 and S1 SAR images under TCs between 2016 and 2021 were collected and later collocated with simultaneous ASCAT winds, with a maximum separation time less than 3.5 h. Note that the corresponding closest-in-time ECMWF IFS model forecasts have been added to the ASCAT WVC positions and are thus contained in the ASCAT data. As a result, one can obtain a triple collocation data set of SAR-ASCAT-ECMWF (SAE). Figure 1a shows the global distribution of SAR images used in this study: there are 47 Radarsat-2 images, 68 Sentinel-1A images, and 33 Sentinel-1B images. Statistically, there are 169 SAR-ASCAT pairs available (some SAR data can match multiple ASCAT images) for imaging TCs, of which TC categories range from tropical storm category to Category 5. TC categories are defined based on the Saffir–Simpson Scale. A collocation between S1 and RS-2 TC images was performed, and a statistical comparison of wind speeds is displayed in Figure 1b. For TC information, refer to Table 1. The statistical results suggest a high consistency between these two SAR wind sources. As such, we can consider that S1 and RS-2 provide similar winds, and hence the intercalibration of NRCS signals can be assumed negligible when the same GMF is used. The statistical results are consistent with the analysis by Zhang et al. (see Figure 3 in [50]), in which comparable wind speeds can be retrieved from these two different SAR missions when using the same GMFs. Furthermore, a series of investigations [6,7,51,52] have demonstrated significant similarities between S1 and

RS-2 NRCS (after calibration) distributions versus wind speeds. The great consistency implies the potential to combine different instrument measurements (e.g., S1 and RS-2 winds used in the study) in service of increasing temporal sampling of TCs.

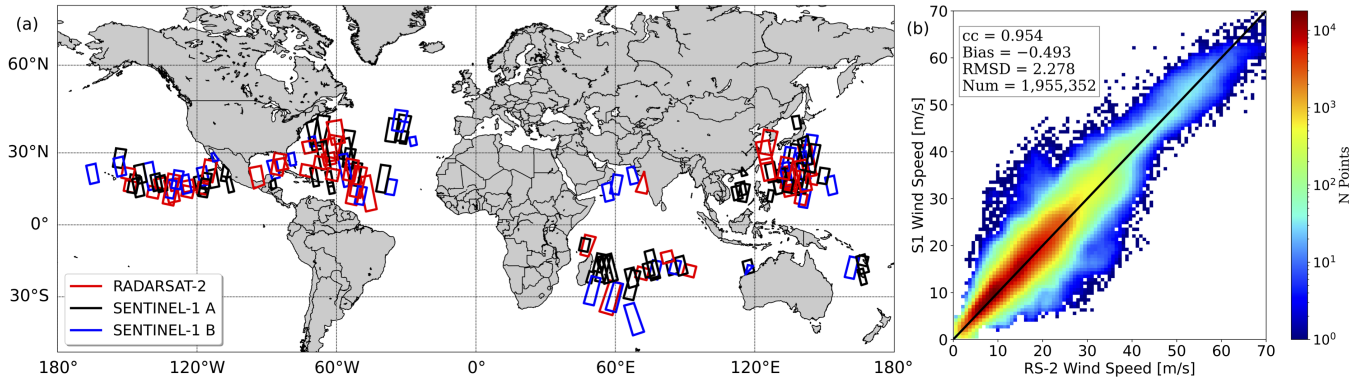

Figure 1. (**a**) The geographic locations of SAR TC images used in this study. Note that simultaneous ASCAT acquisitions with a time departure less than 3.5 h can be found. The red, black, and blue squares denote RS-2, S1-A, and S1-B, respectively. (**b**) Scatter plot of S1 SAR winds versus RS-2 wind speeds, which suggests a high consistency between these two SAR wind sources. Thus, the differences between S1 and RS-2 winds can be assumed negligible when the same GMF is used.

Table 1. SAR Imagery Information of TC cases, wherein both RS-2 and S1 observations are available. Cyclone locations are Eastern Pacific (EPA), Western Pacific (WPA), Atlantic (ATL), and Indian Ocean (IND).

No.	TC Name	Acquisition Time	Cyclone Location	TC Centre	Category
1	KARL	2016-09-23	ATL	(65.2°W, 31.1°N)	1
2	DUMAZILE	2018-03-08	IND	(57.6°E, 29.4°S)	TS
3	JONGDARI	2018-07-24	WPA	(137.2°E, 21.1°N)	1
4	HECTOR	2018-08-07	EPA	(147.9°W, 16.1°N)	4
5	SOULIK	2018-08-18	WPA	(140.1°E, 24.8°N)	2
6	MIRIAM	2018-08-29	EPA	(139.2°W, 14.0°N)	1
7	BELNA	2019-12-07	IND	(47.7°E, 9.3°S)	1
8	MINDULLE	2021-09-25	WPA	(137.0°E, 18.6°N)	4
9	MALOU	2021-10-26	WPA	(139.1°E, 20.7°N)	2

After that, a statistical comparison between SAR- and ASCAT-retrieved wind speeds was carried out and is shown in Figure 2a. Here, the SAR wind speeds are retrieved from dual-polarized signals using the MS1AHW GMF. Three error metrics are adopted: bias, Root Mean Square Difference (RMSD), and Pearson's correlation coefficient (CC). They are expressed in the form of Equations (1)–(3), where x indicates ASCAT wind speed estimates and y indicates the SAR acquisitions. The overbar stands for the mean values.

$$bias = \frac{1}{n}\sum_{i=1}^{n}(y_i - x_i) \tag{1}$$

$$RMSD = \sqrt{\frac{1}{n}\sum_{i=1}^{n}(y_i - x_i)^2} \tag{2}$$

$$CC = \frac{\sum_{i=1}^{n}(y_i - \overline{y})(x_i - \overline{x})}{\sqrt{\sum_{i=1}^{n}(y_i - \overline{y})^2 \sum_{i=1}^{n}(x_i - \overline{x})^2}} \tag{3}$$

Figure 2b presents the wind speed probability distribution functions (PDFs) of three wind systems (SAR, ASCAT, and ECMWF winds), revealing an apparent discrepancy between SAR and ASCAT/ECMWF wind estimates. Figure 2c plots the bias (blue curves)

and standard deviation of difference (SDD) values of individual wind systems with mean winds (the best truth when errors are similar [53], as indicated by the close SDD values at moderate winds) at an interval of 5 m/s. The relatively large SDD differences across three wind systems at high winds are considered to be due to the high sampling uncertainties, $\frac{SDD}{\sqrt{N-1}}$, where N is the count of sampling points. The uncertainty can surge to around 0.5 m/s at extremes (no results shown). For a motivation to use triple collocation and mean values in the computation of SDD, we refer to Appendix A. It can be observed that these three wind systems have similar wind speed estimates for the low-to-moderate wind speed regime ($\leq$14 m/s), wherein the bias values are all close to zero. However, when wind speeds exceed 14 m/s, SAR wind speeds appear overestimated compared to the other two wind sources (which is in line with the recent studies [54,55]) and are the most inconsistent as the SDD values are the largest, though ECMWF is close. As spatial representativeness errors appear low (see Section 4), the enhanced SAR resolution appears not dominant here. Besides spatial variability, random differences contributing to the SDD may emerge from variable calibration, processing, and numerical artefacts. In particular, the poor calibration ($\sim$0.5 dB) of SAR data [56] is perhaps a major element for its high SDD values. The ASCAT winds appear the most consistent. The reported signal saturation phenomenon for VV signals should reduce ASCAT sensitivity and therefore increase its random error. However, as the SDD remains relatively small, this effect appears small as well, cf. [7]. It is also noteworthy here that there exists a high CC value of 0.901, indicating that with an appropriate high-wind-scaling, the ASCAT winds and SAR winds can be made consistent.

Following the wind speed reference de facto used in operational TC advisories, the dropsonde-based SAR winds, on the one hand, and ASCAT and ECMWF winds based on moored buoys, on the other, will be mutually biased at the extremes. The effect of bias correction is investigated. SAR winds are used as the reference to adjust ASCAT CMOD7 and ECMWF winds to align with SAR wind speeds. The behaviour of the dependence between ASCAT (V_{ASCAT}) and SAR winds (V_{SAR}) shown in Figure 2a suggests a parametric model of the form

$$V_{SAR} = a * V_{ASCAT}^{b} - c \tag{4}$$

This parametric model is fit to SAR-ASCAT wind speed collocations using the Least Square approach, with a, b and c as constant real numbers. As a result, the adjustment from ASCAT to SAR winds can be approximated as follows and vice versa:

$$V_{CMOD7D} = 0.88 * V_{CMOD7}^{1.18} - 5.81 \tag{5}$$

where V_{CMOD7} and V_{CMOD7D} indicate the buoy-based wind speed provided to the CMOD7 GMF and the obtained dropsonde-scale wind speeds (since dropsondes are used as the fundamental calibration reference for SAR winds). Notably, the adjustment is only applied to winds with wind speeds higher than 14 m/s.

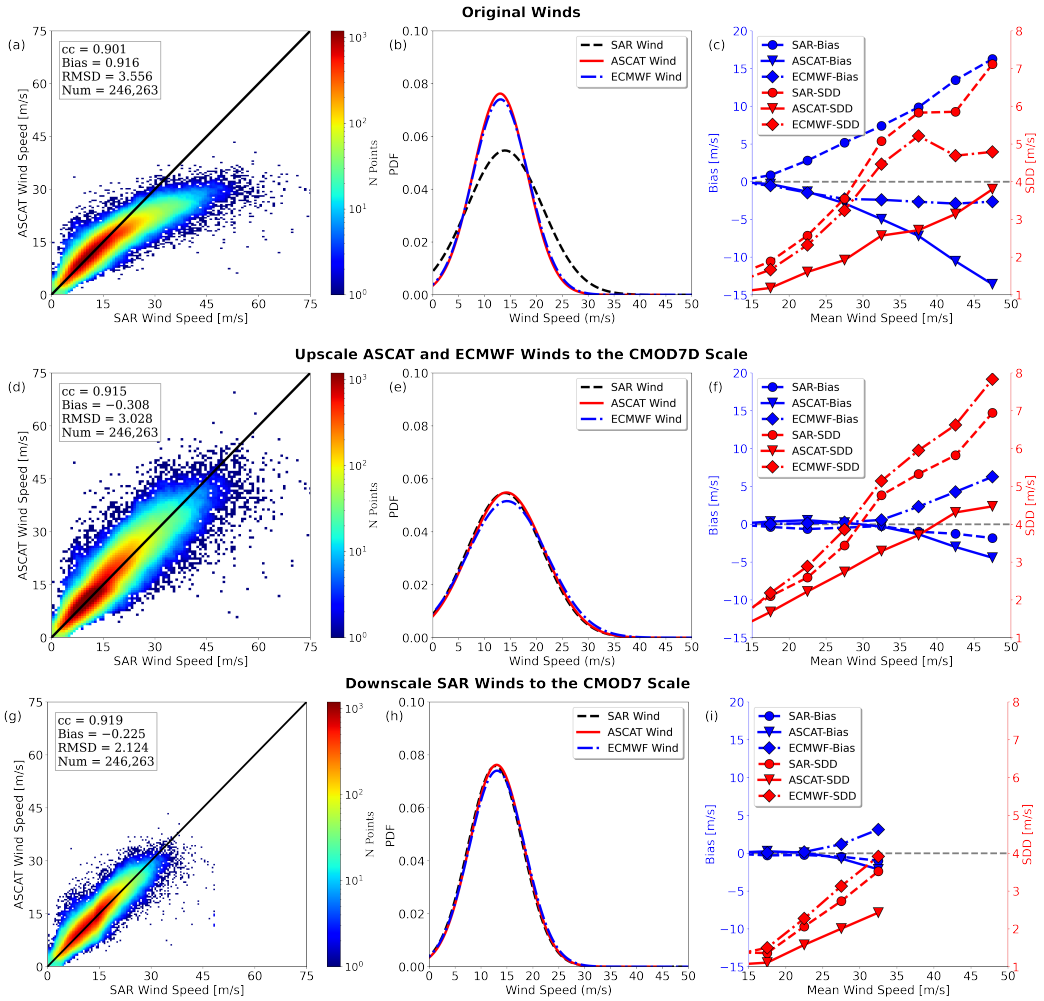

Figure 2. (**Left panels—a**,**d**,**g**): Scatter plots of ASCAT winds versus SAR MS1AHW wind speeds. (**Middle panels—b**,**e**,**h**): Wind-speed PDFs of original/adjusted satellite winds as a function of wind speeds. (**Right panels—c**,**f**,**i**): Bias (**blue curves**) and SDD values (**red curves**) of three wind sources as a function of mean wind speeds. The mean wind speed is considered the best truth when errors are similar; see the close SDD values. The upper panels present the statistical comparison between SAR- and ASCAT-retrieved wind speeds, showing an apparent discrepancy at extremes. The second row of panels presents statistical results with respect to SAR wind speeds when upscaling ASCAT and ECMWF winds to the CMOD7D wind speed scale. The lower panels show the corresponding results when downscaling SAR winds to the CMOD7 wind speed scale. As can be found, the proposed CMOD7D-v2 adjustment can efficiently eliminate the wind speed differences between SAR and ASCAT/ECMWF winds, generating similar wind-speed PDF curves.

4. Results

The study first upscales ASCAT and ECMWF winds to the CMOD7D scale. Figure 2d presents the scatter plot of adjusted ASCAT winds versus SAR winds. Notably, the adjustment reduces the bias from 0.916 m/s to −0.308 m/s and RMSD from 3.556 m/s to 3.028 m/s. Furthermore, a higher CC (0.915) can be obtained. Figure 2e presents wind speed PDFs of SAR, adjusted ASCAT and adjusted ECMWF winds, showing a much higher consistency than the unadjusted ones (Figure 2b). In addition, the mutual biases of these three wind systems (the blue curves in Figure 2f) are significantly reduced, while SDD values remain relatively unchanged. It is notable that after CMOD7D-v2 adjustment, ECMWF forecasts have the highest SDD values, but the values are very close to SDDs of SAR winds due to small-scale variations. Generally, the spatial variability in ECMWF forecasts is reduced by spatial smoothing as ECMWF employs a diffusion operator [57] with

a width beyond the spatial dimension of a TC to control small-scale numerical differentiation error. One would therefore expect both SAR and ASCAT to contain similar small-scale information, while ECMWF winds appear more smooth and thus explode ECMWF SDD values. Indeed, both SAR and ASCAT show structures related to moist convection inflow, while often at different stages of development, due to the time difference of acquisition and fast time scale of moist convection. In addition, SAR winds suffer calibration features and poorer wind vector resolution. The latter causes smooth wind directions in the SAR products used here and hence the correlation between speed and direction retrieval errors. These factors appear to imply a poor correlation between ASCAT and SAR on the smaller ASCAT scales, relatively large SAR errors, and a relatively smooth mean wind field. The smoother ECMWF wind speeds therefore do not deviate too much from the mean in SDD, showing close SDD values to SAR SDDs. The comparison has also been satisfactorily made by downscaling SAR winds to the CMOD7 scale, as illustrated in the third row in Figure 2: the adjustment improves CC with ASCAT by about 2.0% and RMSD by about 40.3%. Notably, the obtained SDD values of SAR winds are smaller with respect to the results shown in Figure 2f, demonstrating that the high random errors of SAR winds at extremes can be significantly reduced by downscaling SAR winds to the CMOD7 scale. Nevertheless, these experimental results illustrate that both moored buoy and dropsonde wind references can be used without biasing to one of them. In addition, ECMWF IFS forecasts show higher wind speeds compared to ASCAT or adjusted SAR winds when mean wind speeds are higher than about 20 m/s; see the positive bias value of ECMWF forecasts in Figure 2i. A similar phenomenon can also be observed in Figure 2f for winds with mean wind speeds higher than 30 m/s. This implies that the development imposed in ECMWF's newly upgraded IFS model [58], despite being beneficial in achieving higher TC maximum surface wind speeds, may cause wind speed overestimation in intense TCs.

It is worth mentioning that the previous adjustment schemes by Polverari et al. (2021) and Chou et al. (2013) have also been tested by adjusting ASCAT and ECMWF winds to the CMOD7D scale, as shown in Figure 3a,b. These two wind-speed adjustment schemes, though both capable of achieving overall wind-speed consistency, show some differences: Chou's adjustment fails to compensate for the wind speed underestimation of ASCAT when wind speeds are higher than around 20 m/s. The blue curve in Figure 3c indicates the wind speed bias of Chou's results by mean winds, which have negative values at extremes. On the other hand, the wind speeds of adjusted ASCAT winds by Polverari-2021 are higher than collocated SAR winds (see the red curve in Figure 3c). Consequently, the proposed CMOD7D-v2 adjustment scheme shows a better performance in SAR and ASCAT wind speed reconciliation, with bias values closer to zero. Polverari-2021 uses SFMR as the reference and does not consider SAR observations. For research involving SAR, ASCAT, and ECMWF winds, the experimental results above suggest that the proposed adjustment can achieve better wind speed consistency across SAR, ASCAT, and ECMWF forecast winds.

Figure 4 presents TCs (the upper for TC Larry, acquired on 7 September 2021; the lower for TC Blas, acquired on 8 July 2016) imaged by adjusted ASCAT and SAR MS1AHW winds. Both these two wind maps show similar band structures. The right panels present wind speed variations along the transects (the black transects in Figure 4) through the TC centres. As can be observed, compared to the original ASCAT CMOD7 winds, the adjusted ASCAT winds are more consistent with SAR estimates, especially for the eyewall area with high gradients.

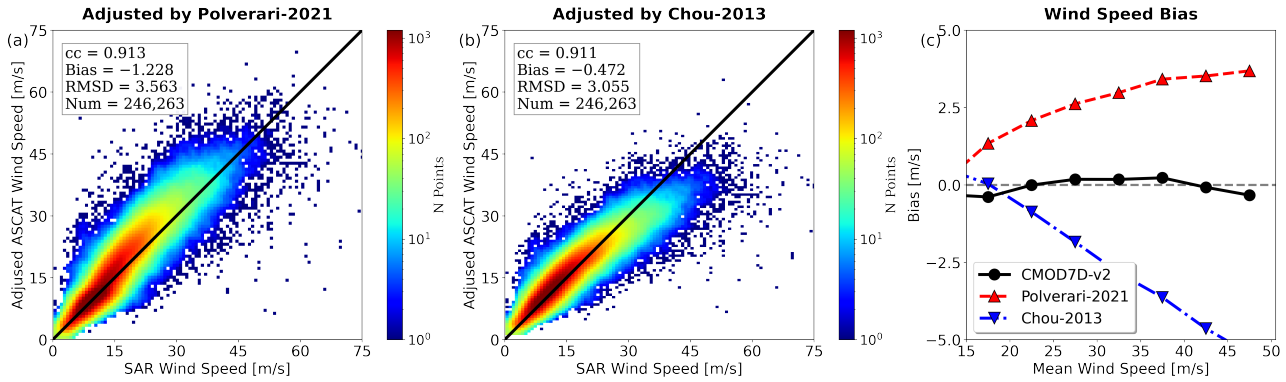

Figure 3. (**a**) Scatter plot of adjusted ASCAT CMOD7 winds (by Polverari-2021) versus SAR MS1AHW winds. (**b**) Scatter plot of adjusted ASCAT CMOD7 winds (by Chou-2013) versus SAR MS1AHW winds. (**c**) Wind speed bias values of three kinds of adjusted ASCAT winds as a function of mean wind speeds. It can be observed that the ASCAT winds adjusted by CMOD7D-v2 have the lowest wind speed bias values.

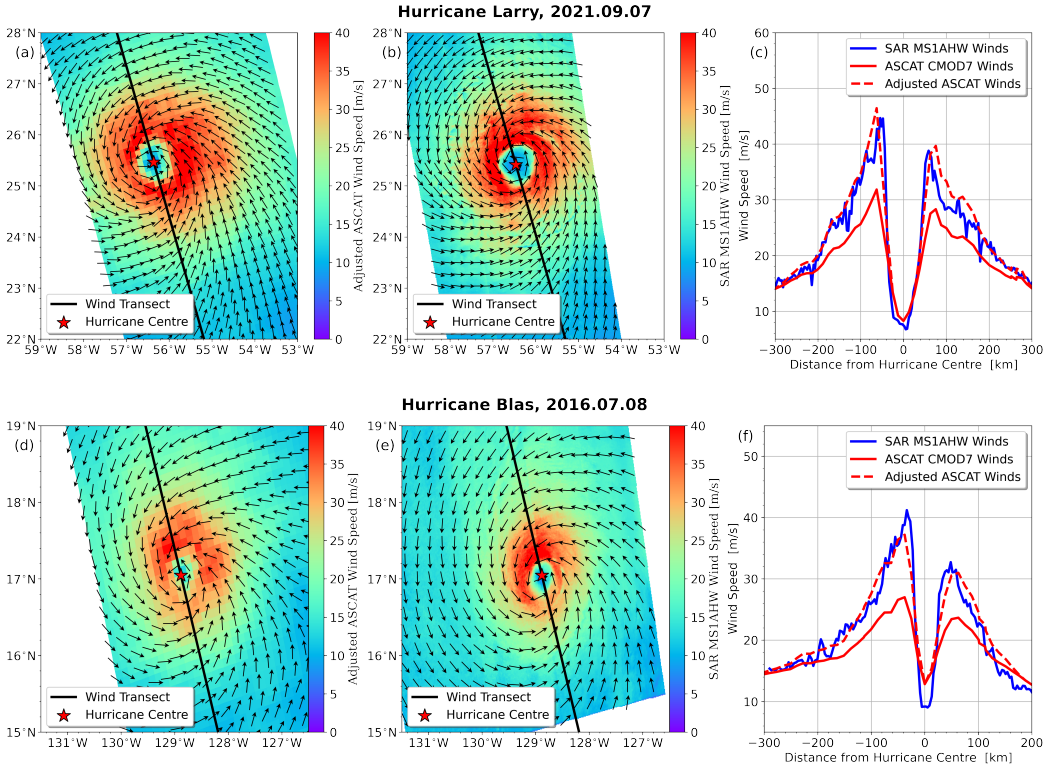

Figure 4. (**Left panels**–**a**,**d**): TC wind fields imaged by adjusted ASCAT CMOD7 wind speeds. (**Middle panels**–**b**,**e**): TC wind field imaged by SAR MS1AHW winds. (**Right panels**–**c**,**f**): The blue and red solid curves indicate the wind speed variations provided by original SAR and ASCAT winds along the transect through the TC centres, showing a large discrepancy, especially around the eyewall with deep gradients. Note that the CMOD7D-v2 adjustment performs well in bridging the gap: the adjusted ASCAT winds (red dashed curves) are close to the SAR ones.

The encouraging consistency among SAR, ASCAT, and ECMWF winds after CMOD7D-v2 adjustment makes it possible to adopt the triple collocation technique [28] to estimate uncertainties and errors of these wind systems. The triple collocation technique can simultaneously calculate the error variance estimates of each source and relative calibration coefficients, given a set of triplets of the variable of interest (e.g., the wind speed triplet of SAE is used here) and assuming linear calibration. Suppose three wind measurements, w_i,

i = 1,2,3, providing collocated measurements of the same quantity t; then, the measurements and measurement errors can be approximated as

$$w_i = a_i(t + \varepsilon_i) + b_i \tag{6}$$

where t indicates the common part of the measurements; a_i and b_i represent the calibration scaling and bias, respectively; and ε_i stands for the random measurement error in each system, assumed unbiased and uncorrelated to each other. Note that the error variances are assumed to be constant over the range of measured values, and thus:

$$< {\varepsilon_i}^2 >= {\sigma_i}^2,\ i = 1,2,3 \tag{7}$$

Reference [59] has illustrated that error variances can be calculated as:

$${\sigma_1}^2 = C_{11} - \frac{C_{13}(C_{12} - a_2 r^2)}{C_{23}},\ {\sigma_2}^2 = C_{22} - \frac{C_{23}(C_{12} - a_2 r^2)}{C_{13}},\ {\sigma_3}^2 = C_{33} - \frac{C_{23}C_{13}}{C_{12} - a_2 r^2} \tag{8}$$

where r^2 indicates representativeness errors. Covariance $C_{\alpha\beta}$ is defined combining first moment M_α, M_β, and mixed second moment $M_{\alpha\beta}$ as:

$$C_{\alpha\beta} = M_{\alpha\beta} - M_\alpha M_\beta, \quad \alpha, \beta = 1,2,3 \tag{9}$$

For the derivation of error variances, we refer to [59]. For this analysis, the SAR (w_1), ASCAT (w_2), and ECMWF forecast (w_3) winds are used, where w_1 is the reference system with respect to which systems w_2 and w_3 are to be calibrated. The triple collocation analysis for wind triplets SAE is performed at different wind speed regimes: (1) $\leq$ 14 m/s; (2) $>$ 14 m/s; (3) the whole wind speed regime. A 4-sigma test is performed during the triple collocation iterative process, and about 2.5% of collocations are filtered out. As discussed in [60,61], accurate spatial representativeness errors (r^2) are useful when evaluating the individual uncertainties and errors of each collocated data set using triple collocation analysis. Such an error originates from the resolution differences between the various observing systems, representing the short-scale details resolved by SAR and ASCAT but unresolved by ECMWF winds. The r^2 is determined following the ideas in [62,63] by searching for r^2 value where the spread in the error standard deviations (SDs) of three systems reach the minimum. The obtained error SDs of wind-speed triplets (wherein ASCAT and ECMWF winds have been upscaled accordingly) regarding varying r^2 values are shown in Figure 5. The gray dashed lines indicate the optimal r^2 values, where three wind systems are the most consistent. The obtained r^2 values are listed in the last column in Table 2.

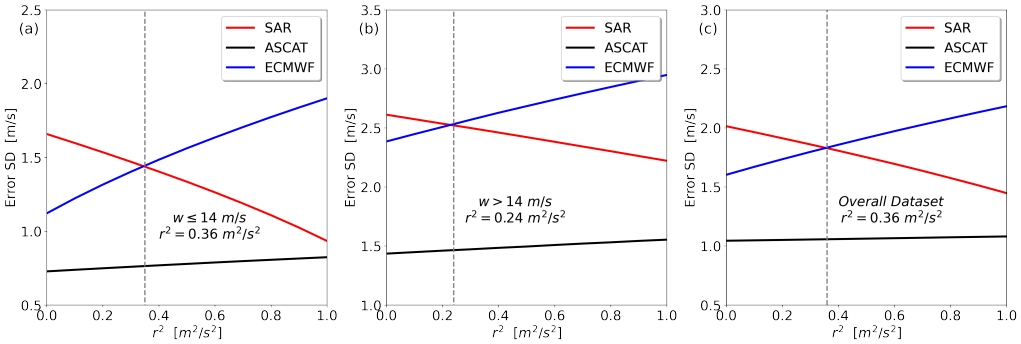

Figure 5. Error SDs of SAR, adjusted ASCAT, and adjusted ECMWF winds under different representativeness errors (r^2). (**a**) for $\leq$ 14 m/s; (**b**) for > 14 m/s, and (**c**) for the whole wind speed regime. The optimal representativeness error is determined when the spread in observation error SDs reach the minimum—see the gray dashed lines.

Table 2. Triple collocation error SDs (m/s) for wind speed (w). The values in parentheses indicate the error improvements after CMOD7D-v2 adjustment.

Wind Speed Regime	Operation	SAR	ASCAT	ECMWF	Representativeness Error (r^2)
≤14 m/s	Not Adjusted [1]	1.43	0.76	1.45	0.36
>14 m/s	Upscale [2]	2.52 (−0.29)	1.47 (−0.28)	2.53 (−0.30)	0.24 (+0.02)
	Downscale [3]	1.63 (−1.18)	1.01 (−0.74)	1.65 (−1.18)	0.05 (−0.17)
	Not Adjusted	2.81	1.75	2.83	0.22
Overall Dataset	Upscale	1.83 (−0.16)	1.06 (−0.12)	1.83 (−0.17)	0.36 (−0.24)
	Downscale	1.49 (−0.50)	0.85 (−0.33)	1.51 (−0.49)	0.24 (−0.36)
	Not Adjusted	1.99	1.18	2.00	0.60

[1] Original SAR, ASCAT and ECMWF wind speeds; [2] ASCAT and ECMWF wind speeds are upscaled to the CMOD7D scale; [3] SAR wind speeds are converted to the CMOD7 scale.

Table 2 lists the obtained error SDs of wind speeds (ε_w). The "Upscale Operation" in the second column indicates that ASCAT and ECMWF wind speeds are upscaled to the CMOD7D scale, while the "Downscale Operation" means the SAR winds are downscaled accordingly. Finally, "Not Adjusted" means all three wind systems remain at their original wind speeds. The r^2 value of 0.36 m^2/s^2 at the moderate wind speed regime (≤14 m/s) is close to the values for lateral and transverse (u, v) wind components reported in [16] and [62], in which the triple collocation analyses are mainly operated at mild wind conditions. It is worth mentioning that the proposed CMOD7D-v2 adjustment can effectively decrease the r^2 values and the subsequent error SDs of the three wind systems in either conversion direction (see the negative values in parentheses in Table 2). Taking the high wind speed regime (>14 m/s) as an example, converting ASCAT and ECMWF winds to the CMOD7D scale can bring in 16.0% and 10.6% improvement in error SDs of ASCAT and ECMWF winds, respectively. The minor increase in r^2 value (+0.02 m^2/s^2) is due to the amplification of random errors. Comparably, when downscaling SAR winds to the CMOD7 scale, the proposed CMOD7D-v2 adjustment can reduce r^2 by 0.17 m^2/s^2 and decrease the error SDs of ASCAT from 1.75 m/s to 1.01 m/s, i.e., an improvement of 42.3%. These improvements suggest that the proposed wind-speed adjustment can help alleviate the wind speed differences across these three wind systems and thus achieve wind speed reconciliation.

Although wind-speed results are reported above, we note a problem in SAR wind direction retrieval: the wind directions in MS1AHW GMF are not determined based on the wind streaks contained in the image but closely associated with collocated ECMWF winds. As a result, the SAR and ECMWF wind directions are both smooth, while ASCAT winds contain more true wind-direction variance. It results in poor statistical results for ASCAT (u, v) wind components in triple collocation analysis: ASCAT winds often have the highest ε_u and ε_v values but the smallest ε_w values (no results shown). It is possible to improve the current SAR wind direction fields using the 2DVAR scheme and further analyze the (u, v) wind components with triple collocation. However, it is beyond the scope of this paper and will be the subject of future research.

5. Discussion

The experimental results in Section 4 show the consistency of the CMOD7D-v2 adjustment between ASCAT CMOD7 winds and dropsonde-based SAR wind speeds, despite the fact that the ASCAT wind speed information is smoothed by its 25-km true spatial resolution of ASCAT [64], reducing the extremes. Objectively, this suggests that the proposed statistical CMOD7D-v2 adjustment matches km-scale SAR winds with 25 km scale ASCAT winds and with ECMWF winds, assigning specific spatial resolution (SAR) or the lack thereof (ECMWF) as noise contributions. This section aims to further validate

the consistency of the CMOD7D-v2 adjustment, excluding the impacts of blurring effects on adjustment results. As the wind speed reconciliations in CMOD7 (i.e., the "Downscale" operation in Table 2) and CMOD7D scales (the "Upscale" operation) display similar improvements, the study here only presents the results when scaling CMOD7 winds to CMOD7D. In addition, a comprehensive discussion on the merits and limitations of the new adjustment is included in this section.

5.1. Tests between SAR VV- and Dual-Polarized Wind Speeds

The dual-polarization mode of SARs enables it to make a direct comparison between VV wind and dual-polarized wind estimates and thus assist the evaluation of the CMOD7D-v2 adjustment for high spatial resolution images. Note that the existing studies [65,66] have shown that the GMFs developed from C-band scatterometer observations can be directly applied to SAR data. As such, this study first retrieved the wind speeds from SAR VV signals using CMOD7 GMF (acting as a substitute for ASCAT winds but with grid size of around 1 km) and then adjusted them with Equation (5) accordingly (named CMOD7D winds here). The scatter plots of SAR CMOD7/CMOD7D winds versus SAR MS1AHW winds (retrieved from dual-polarized signals) are shown in Figure 6a,b. For SAR CMOD7D winds, a higher CC (0.946) and lower bias (0.708 m/s), along with a lower RMSD (2.113 m/s), can be obtained with regard to original SAR CMOD7 winds shown in Figure 6a, wherein CC is 0.942, bias is 1.357 m/s, and RMSD is 2.587 m/s.

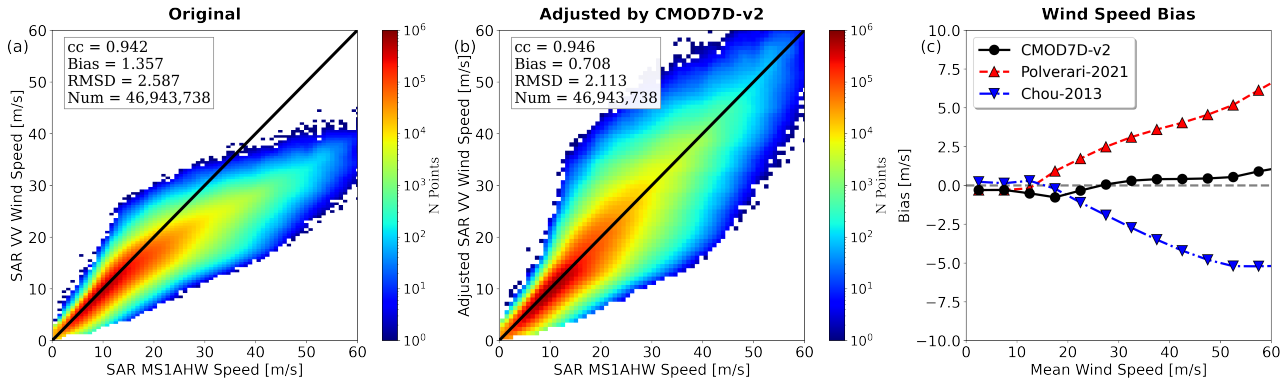

Figure 6. (**a**) SAR VV wind speeds (retrieved with CMOD7 GMF) versus SAR MS1AHW estimates (calculated from dual-polarized signals). (**b**) Adjusted SAR VV wind speeds versus SAR MS1AHW estimates. (**c**) The bias values of CMOD7D wind speeds (by three wind-adjustment schemes) as a function of mean wind speed. The black, red, and blue curves indicate the corresponding results of the proposed CMOD7D-v2, Polverari-2021 and Chou-2013, respectively. As can be observed, the CMOD7D-v2 adjustment has smaller bias values over the whole wind-speed regime.

The other two adjustment schemes (Polverari-2021 and Chou-2013) for SAR CMOD7 wind speed adjustments were also employed to calculate the speed bias at an interval of 5 m/s of mean wind speeds (estimated by SAR MS1AHW winds and obtained SAR CMOD7D winds by three adjustment schemes), as shown in Figure 6c. Figure 6c shows that the CMOD7D-v2 adjustment has a lower bias error (by around 5 m/s) for the high wind speed regime, while Polverari-2021 and Chou-2013 may overestimate/underestimate winds. This suggests that the effect of spatial resolution differences between SAR and ASCAT on earlier results (Figure 3) is small. This may be explained by the earlier assertion that the "mean" truth effectively used in this manuscript does not contain the smallest scales. These are rather represented in the SAR SDDs. As the ASCAT SDDs are smaller and relatively insensitive to the spatial representativeness error, one might deduce that the triple collocation results are most applicable to the scatterometer-resolved spatial scales. From this section, it may subsequently be concluded that changes to the GMF obtained at scatterometer scales are applicable at SAR-observed scales. In other words, the geophysical relationships (GMF) are not strongly spatial-scale dependent, but rather,

the higher resolution sensors will observe more detail and hence higher NRCS and more extreme wind speeds in TCs. Therefore, scatterometer-based GMFs are applied successfully for SAR-retrieved winds.

5.2. Tests between SAR VV Winds and SFMR Observations

The relevant verification and analysis are further extended by comparing the obtained SAR CMOD7 winds to simultaneous SFMR measurements. For this purpose, historical SAR images are collocated with SFMR tracks. There are 156 SFMR tracks available in total. The collocated SFMR tracks between 2014 and 2021 for individual SAR sensors (S1-A, S1-B and RS-2) are listed in Table 3. The scatter plots of SAR CMOD7/CMOD7D winds versus collocated SFMR wind measurements averaged over a distance of 1 km along the tracks are shown in Figure 7a/Figure 7b. Note that only the collocations with time departures Δt less than 3 h are selected.

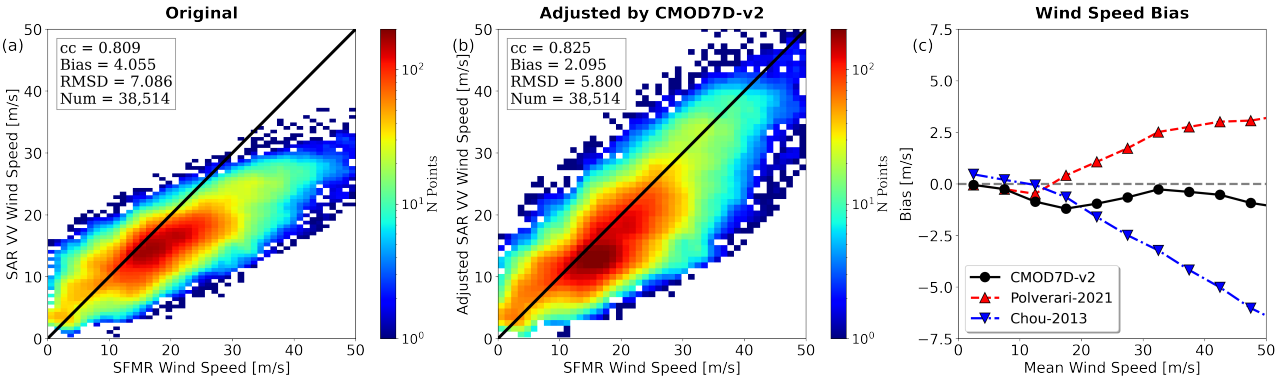

Figure 7. (**a**) SAR VV wind speeds (retrieved with CMOD7 GMF) versus SFMR measurements. (**b**) Adjusted SAR VV wind speeds versus SFMR measurements. (**c**) The bias values of CMOD7D wind speeds (by three wind-adjustment schemes) as a function of mean wind speed. The black, red, and blue curves indicate the corresponding results of the proposed CMOD7D-v2, Polverari-2021 and Chou-2013, respectively. As can be observed, the CMOD7D-v2 adjustment has smaller bias values over the whole wind-speed regime.

Table 3. The number of SFMR tracks collocated with Sentinel-1 A (S1-A), Sentinel-1B (S1-B), and Radarsat-2 (RS-2) TC images between 2014 and 2021.

Year	S1-A	S1-B	RS-2	Sum of Tracks
2014	2	0	8	10
2015	0	0	12	12
2016	10	2	5	17
2017	9	5	9	23
2018	8	9	10	27
2019	23	5	2	30
2020	13	13	17	43
2021	0	1	2	3

The known deviation between SFMR and CMOD7 winds is evident. As before, when adjusting SAR CMOD7 estimates to obtain CMOD7D winds, the correspondence improves. The obtained SAR CMOD7D winds can obtain values up to 50 m/s at good quality, reducing bias from 4.055 m/s to 2.095 m/s and RMSD from 7.086 m/s to 5.8 m/s. In addition, the adjustment can improve CC by about 2.0%. It is worth noting that the scatter plot of SAR winds versus SFMR observations shows a higher spread compared to that in the scatter plot of SAR winds versus ASCAT (Figure 2d) and that in the scatter plot of SAR CMOD7 winds versus SAR MS1AHW winds (Figure 6a), especially at the low-to-moderate wind speed regime (<14 m/s). It hinders convergence in triple collocation analysis and thus

makes it difficult to achieve an accurate estimation of wind speed errors. One cause of the severe spread across SAR and SFMR winds is supposed to be the noise and high variations contained in SFMR observations. This agrees with current discussions on the quality issues of SFMR observations, as introduced in the Introduction.

Furthermore, the bias values of obtained CMOD7D winds and counterparts by the other two adjustment schemes are calculated as a function of mean wind speed at an interval of 5 m/s, as shown in Figure 7c. The horizontal coordinate indicates the average wind speed of SAR MS1AHW, CMOD7D winds, and SFMR estimates. Similar to the results presented in Section 5.1, the proposed CMOD7D-v2 adjustment shows a lower bias value compared to other two adjustments (by up to 5 m/s) at the most extreme values.

5.3. Limitations and Future Research

The experiments above demonstrate the capability of the proposed wind-adjustment scheme in achieving wind-speed consistency across different wind sources. Moreover, compared to the existing two wind-adjustment schemes, the proposed one has lower bias values over the whole wind-speed regime. Nevertheless, it should be noted that all these wind adjustments are constructed based on the differences between different GMF retrievals, which intrinsically originate from the deviations between wind reference bases selected (e.g., moored buoy and dropsonde introduced in the study). In real conditions, the wind speed retrieval differences between various satellite instruments can be related to other factors, such as the impacts of processing. Taking Figure 6 as an example, although the obtained CMOD7D winds have a similar distribution trend with regard to SAR MS1AHW winds, a large spread across the observations can be observed at the high wind-speed regime (e.g., > 20 m/s), which illustrates the impacts of these other factors. As such, the proposed CMOD7D-v2 adjustment scheme, as well as the other two wind adjustments, are capable of achieving an overall statistical wind speed reconciliation but may not capture the full extreme variability conditions. Therefore, a more subtle wind adjustment scheme is expected to be constructed in future research with more factors taken into account in terms of physics, processing, and representation.

6. Conclusions

Since the birth of space-borne active microwave sensors, a series of GMFs have been developed to detect ocean surface winds with increasing accuracy. However, the reliability of wind references bases deserves doubt and satellite wind mutual adjustment at extremes is necessary to improve the usefulness of available satellite records. Therefore, exploring the relationship between different GMF retrievals can be conducive to the long-term goal of building a more consolidated wind reference for the whole wind speed regime in the future. The study builds a new CMOD7D-v2 adjustment based on the wind speed differences between ASCAT CMOD7 and SAR MS1AHW winds. The experimental results confirm that the adjustment is effective and can achieve a good wind speed reconciliation across different wind sources. In particular, the triple collocation analysis results suggest that the errors of ASCAT winds can be reduced by around 16.0% (42.3%) when scaling ASCAT and ECMWF winds (SAR winds) to the CMOD7D (CMOD7) scale following the adjustment, efficiently alleviating the wind speed differences across wind sources. Furthermore, the proposed scheme has lower bias values (by around 5 m/s) at the most extreme values than the existing wind-adjustment schemes.

More TC cases will be added in future research to provide further and more accurate results. In addition, the feasibility of CMOD7D-v2 adjustment implies that the triple collocation analysis for wind triplets of SAE (i.e., wind triplet of SAR-ASCAT-ECMWF introduced in Section 3) is credible and thus can provide more reasonable background (e.g., ECMWF forecasts) and observation (e.g., SAR and ASCAT observations) error SDs. It will benefit the data assimilation of ASCAT data in TC cases. However, more factors need to be considered, such as the observation density and quality issues. As such, a stricter quality control scheme is required for subsequent research. Finally, consolidated SAR, ASCAT and

ECMWF wind speeds will be helpful for 2DVAR studies into ASCAT TC winds resolution enhancement.

Author Contributions: Methodology and investigations: W.N.; software: A.S. and J.V.; writing—original draft preparation: W.N.; writing—review and editing: all authors; supervision: A.S., K.R., X.Y., and J.V. All authors have read and agreed to the published version of the manuscript.

Funding: This work was partially supported by the National Key Research and Development Program of China under Grant No. 2018YFB0203801 and the National Natural Science Foundation of China under Grant Nos. 61702529 and 61802424. This work was also partially supported by the science and technology innovation program of Hunan Province under Grant No. 2022RC3070. Ad Stoffelen and Jur Vogelzang are supported by the EUMETSAT OSI SAF.

Data Availability Statement: The SAR data are archived by Institut Français de Recherche pour l'Exploitation de la Mer (IFREMER) and are publicly available. This dataset can be found at https://cyclobs.ifremer.fr/app/tropical (accessed on 4 May 2022). SFMR data are available from NOAA website (https://www.aoml.noaa.gov/hrd/data_sub/hurr.html, accessed on 4 May 2022). The ASCAT data in BUFR and NetCDF format can be ordered online from the EUMETSAT Data Centre, https://www.eumetsat.int/eumetsat-data-centre (accessed on 4 May 2022). They are also available from PO.DAAC (https://podaac.jpl.nasa.gov/datasetlist?values=ASCAT&view=list&ids=Instruments, NetCDF format only) (accessed on 4 May 2022). The Geophysical Model Function (GMF) CMOD7 is available at https://scatterometer.knmi.nl/cmod7/ (accessed on 4 May 2022).

Acknowledgments: Most datasets used in this study are provided by the EUMETSAT OSI SAF. The authors acknowledge ESA and IFREMER for SAR data obtained through SHOC and support through the MAXSS project.

Conflicts of Interest: No potential conflict of interest was reported by the authors.

Appendix A. The Bias Values and Standard Deviation of Difference with Regard to Mean Values

Here, we discuss the estimation of random errors of triple collocations of observation systems, x_i, with i the observation system index, $i = 1, 2, 3$. Assuming there are no remaining biases, we can define the measurements of wind observation system x_i as:

$$x_1 = t + \varepsilon_1 \tag{A1}$$

$$x_2 = t + \varepsilon_2 \tag{A2}$$

$$x_3 = t + \varepsilon_3 \tag{A3}$$

$$m = t + (\varepsilon_1 + \varepsilon_2 + \varepsilon_3)/3 \tag{A4}$$

where t indicates the common part of the signal (sometimes referred to as the "truth") and ε_i is the random error in each measurement with variance ${\sigma_i}^2$. It is also assumed that ε_i values are uncorrelated with each other, $\langle \varepsilon_i \varepsilon_j \rangle = 0$, $i \neq j$, nor with the common signal t, $\langle t \varepsilon_i \rangle = 0$. m indicates the mean value.

Hence, for observation system of x_1, the differences with m can be expressed as:

$$x_1 - m = \varepsilon_1 - \frac{(\varepsilon_1 + \varepsilon_2 + \varepsilon_3)}{3} \tag{A5}$$

$$Bias = \frac{\sum_{j=1}^{N} (x_1^j - m^j)}{N} \tag{A6}$$

where j is the collocation index, $j = 1, \ldots, N$. Subsequently, when bias is ignored, the standard deviation of difference (SDD) of observation system x_1 (SDD_1) can be obtained in the form of:

$$SDD_1 = \frac{1}{N}\sqrt{\sum_{j=1}^{N}(x_1 - m)^2} = \frac{2}{3}\sqrt{\sigma_1 + \frac{\sigma_2}{4} + \frac{\sigma_3}{4}} \tag{A7}$$

The lowest SDD value implies the lowest random error and hence the largest consistency with t. The SDD values for x_2 and x_3 can be calculated in the same way. For comparison, assuming double collocations of observation systems, x_1 and x_2, in which x_2 is used as the reference data, one can obtain the SDD of x_1 as:

$$SDD_1 = \frac{1}{2}\sqrt{\sigma_1 + \sigma_2} \tag{A8}$$

As can be inferred, σ_1 can only be properly calculated with knowledge of the error characteristics of reference data, σ_2. However, prior knowledge of complete error properties is seldom available in practice. As such, the SDD calculation with respect to the mean m from, at least, triple collocatioins is a more reasonable estimate of the random error of observation system x_i.

References

1. Hersbach, H.; Stoffelen, A.; de Haan, S. An improved C-band scatterometer ocean geophysical model function: CMOD5. *J. Geophys. Res. Ocean* **2007**, *112*. [CrossRef]
2. Hwang, P.A.; Stoffelen, A.; van Zadelhoff, G.J.; Perrie, W.; Zhang, B.; Li, H.; Shen, H. Cross-polarization geophysical model function for C-band radar backscattering from the ocean surface and wind speed retrieval. *J. Geophys. Res. Ocean* **2015**, *120*, 893–909. [CrossRef]
3. Zhang, G.; Li, X.; Perrie, W.; Hwang, P.A.; Zhang, B.; Yang, X. A hurricane wind speed retrieval model for C-band RADARSAT-2 cross-polarization ScanSAR images. *IEEE Trans. Geosci. Remote Sens.* **2017**, *55*, 4766–4774. [CrossRef]
4. Mouche, A.A.; Chapron, B.; Zhang, B.; Husson, R. Combined co-and cross-polarized SAR measurements under extreme wind conditions. *IEEE Trans. Geosci. Remote Sens.* **2017**, *55*, 6746–6755. [CrossRef]
5. Stoffelen, A.; Verspeek, J.A.; Vogelzang, J.; Verhoef, A. The CMOD7 geophysical model function for ASCAT and ERS wind retrievals. *IEEE J. Sel. Top. Appl. Earth Obs. Remote Sens.* **2017**, *10*, 2123–2134. [CrossRef]
6. Mouche, A.; Chapron, B.; Knaff, J.; Zhao, Y.; Zhang, B.; Combot, C. Copolarized and Cross-Polarized SAR Measurements for High-Resolution Description of Major Hurricane Wind Structures: Application to Irma Category 5 Hurricane. *J. Geophys. Res. Ocean* **2019**, *124*, 3905–3922. [CrossRef]
7. Stoffelen, A.; Mouche, A.A.; Polverari, F.; van Zadelhoff, G.J.; Sapp, J.; Portabella, M.; Chang, P.; Lin, W.; Jelenak, Z. C-band High and Extreme-Force Speeds (CHEFS)—Final Report. 2020. Available online: http://hdl.handle.net/10261/222000 (accessed on 4 May 2022).
8. Knaff, J.A.; Sampson, C.R.; Kucas, M.E.; Slocum, C.J.; Brennan, M.J.; Meissner, T.; Ricciardulli, L.; Mouche, A.; Reul, N.; Morris, M.; et al. Estimating tropical cyclone surface winds: Current status, emerging technologies, historical evolution, and a look to the future. *Trop. Cyclone Res. Rev.* **2021**, *10*, 125–150. [CrossRef]
9. Large, W.; Crawford, G. Observations and simulations of upper-ocean response to wind events during the ocean storms experiment. *J. Phys. Oceanogr.* **1995**, *25*, 2831–2852. [CrossRef]
10. Zeng, L.; Brown, R.A. Scatterometer observations at high wind speeds. *J. Appl. Meteorol.* **1998**, *37*, 1412–1420. [CrossRef]
11. Stoffelen, A.; Marseille, G.J.; Ni, W.; Mouche, A.; Polverari, F.; Portabella, M.; Lin, W.; Sapp, J.; Chang, P.; Jelenak, Z. Hurricane ocean wind speeds. In Proceedings of the 2021 IEEE International Geoscience and Remote Sensing Symposium IGARSS, Brussels, Belgium, 11–16 July 2021; pp. 1182–1185.
12. Wright, E.E.; Bourassa, M.A.; Stoffelen, A.; Bidlot, J.R. Characterizing Buoy Wind Speed Error in High Winds and Varying Sea State with ASCAT and ERA5. *Remote Sens.* **2021**, *13*, 4558. [CrossRef]
13. Sapp, J.W.; Alsweiss, S.O.; Jelenak, Z.; Chang, P.S.; Carswell, J. Stepped Frequency Microwave Radiometer Wind-Speed Retrieval Improvements. *Remote Sens.* **2019**, *11*, 214. [CrossRef]
14. Polverari, F.; Sapp, J.W.; Portabella, M.; Stoffelen, A.; Jelenak, Z.; Chang, P.S. On dropsonde surface-adjusted winds and their use for the Stepped Frequency Microwave Radiometer wind speed calibration. *IEEE Trans. Geosci. Remote Sens.* **2022**, *60*, 4208308. [CrossRef]
15. Stoffelen, A.; Mouche, A.A.; Polverari, F.; van Zadelhoff, G.J.; Sapp, J.; Portabella, M.; Chang, P.; Lin, W.; Jelenak, Z. *An In-Situ Reference for High and Extreme Winds*; European Geosciences Union: Vienna, Austria, 2020.
16. Polverari, F.; Portabella, M.; Lin, W.; Sapp, J.W.; Stoffelen, A.; Jelenak, Z.; Chang, P.S. On High and Extreme Wind Calibration Using ASCAT. *IEEE Trans. Geosci. Remote Sens.* **2021**, *60*, 4202210. [CrossRef]
17. Verhoef, A.; Vogelzang, J.; Verspeek, J.; Stoffelen, A. Long-term scatterometer wind climate data records. *IEEE J. Sel. Top. Appl. Earth Obs. Remote Sens.* **2017**, *10*, 2186–2194. [CrossRef]
18. Young, I.R.; Ribal, A. Multiplatform evaluation of global trends in wind speed and wave height. *Science* **2019**, *364*, 548–552. [CrossRef]
19. Young, I.R.; Kirezci, E.; Ribal, A. The global wind resource observed by scatterometer. *Remote Sens.* **2020**, *12*, 2920. [CrossRef]
20. Ribal, A.; Young, I.R. Calibration and cross validation of global ocean wind speed based on scatterometer observations. *J. Atmos. Ocean. Technol.* **2020**, *37*, 279–297. [CrossRef]

21. Mendeley Data, V. Calibration of Reanalysis Data in the Atlantic Ocean Using Satellite Data, 2022. Available online: https://data.mendeley.com/datasets/tkf74fy9wh (accessed on 4 May 2022).
22. Campos, R.M.; Gramcianinov, C.B.; de Camargo, R.; da Silva Dias, P.L. Assessment and Calibration of ERA5 Severe Winds in the Atlantic Ocean Using Satellite Data. *Remote Sens.* **2022**, *14*, 4918. [CrossRef]
23. Zhang, B.; Perrie, W.; Zhang, J.A.; Uhlhorn, E.W.; He, Y. High-resolution hurricane vector winds from C-band dual-polarization SAR observations. *J. Atmos. Ocean. Technol.* **2014**, *31*, 272–286. [CrossRef]
24. Chou, K.H.; Wu, C.C.; Lin, S.Z. Assessment of the ASCAT wind error characteristics by global dropwindsonde observations. *J. Geophys. Res. Atmos.* **2013**, *118*, 9011–9021. [CrossRef]
25. Tamizi, A.; Young, I.R.; Ribal, A.; Alves, J.H. Global scatterometer observations of the structure of tropical cyclone wind fields. *Mon. Weather. Rev.* **2020**, *148*, 4673–4692. [CrossRef]
26. Holland, G.J.; Belanger, J.I.; Fritz, A. A revised model for radial profiles of hurricane winds. *Mon. Weather. Rev.* **2010**, *138*, 4393–4401. [CrossRef]
27. Ribal, A.; Tamizi, A.; Young, I.R. Calibration of scatterometer wind speed under hurricane conditions. *J. Atmos. Ocean. Technol.* **2021**, *38*, 1859–1870. [CrossRef]
28. Stoffelen, A. Toward the true near-surface wind speed: Error modeling and calibration using triple collocation. *J. Geophys. Res. Ocean* **1998**, *103*, 7755–7766. [CrossRef]
29. Vogelzang, J.; Stoffelen, A.; Verhoef, A.; De Vries, J.; Bonekamp, H. Validation of two-dimensional variational ambiguity removal on SeaWinds scatterometer data. *J. Atmos. Ocean. Technol.* **2009**, *26*, 1229–1245. [CrossRef]
30. Vogelzang, J. *Estimation of Background Error Correlation Functions*; Technical Report, NWPSAF-KN-TR-023 Version 1.0; KNMI: De Bilt, The Netherlands, 2014.
31. Vogelzang, J.; Stoffelen, A. Improvements in Ku-band scatterometer wind ambiguity removal using ASCAT-based empirical background error correlations. *Q. J. R. Meteorol. Soc.* **2018**, *144*, 2245–2259. [CrossRef]
32. Isaksen, L.; Stoffelen, A. ERS scatterometer wind data impact on ECMWF's tropical cyclone forecasts. *IEEE Trans. Geosci. Remote Sens.* **2000**, *38*, 1885–1892. [CrossRef]
33. Yu, Y.; Yang, X.; Zhang, W.; Duan, B.; Cao, X.; Leng, H. Assimilation of sentinel-1 derived sea surface winds for typhoon forecasting. *Remote Sens.* **2017**, *9*, 845. [CrossRef]
34. Duong, Q.P.; Langlade, S.; Payan, C.; Husson, R.; Mouche, A.; Malardel, S. C-band SAR Winds for Tropical Cyclone monitoring and forecast in the South-West Indian Ocean. *Atmosphere* **2021**, *12*, 576. [CrossRef]
35. CSA. RadarSat-2. 2021. Available online: https://www.asc-csa.gc.ca/eng/satellites/radarsat2/what-is-radarsat2.asp. (accessed on 4 May 2022).
36. ESA. Sentinel-1. Available online: https://www.esa.int/Applications/Observing_the_Earth/Copernicus/Sentinel-1/Introducing_Sentinel-1/ (accessed on 4 May 2022).
37. Van Zadelhoff, G.J.; Stoffelen, A.; Vachon, P.; Wolfe, J.; Horstmann, J.; Belmonte Rivas, M. Retrieving hurricane wind speeds using cross-polarization C-band measurements. *Atmos. Meas. Tech.* **2014**, *7*, 437–449. [CrossRef]
38. Zhang, G.; Perrie, W.; Li, X.; Zhang, J.A. A hurricane morphology and sea surface wind vector estimation model based on C-band cross-polarization SAR imagery. *IEEE Trans. Geosci. Remote Sens.* **2016**, *55*, 1743–1751. [CrossRef]
39. Zhang, B.; Mouche, A.A.; Perrie, W. First Quasi-Synchronous Hurricane Quad-Polarization Observations by C-Band Radar Constellation Mission and RADARSAT-2. *IEEE Trans. Geosci. Remote Sens.* **2022**, *60*, 1–10. [CrossRef]
40. Li, X. The first Sentinel-1 SAR image of a typhoon. *Acta Oceanol. Sin.* **2015**, *34*, 1–2. [CrossRef]
41. OSI SAF/EARS Winds Team. ASCAT Wind Product User Manual. Version 1.16. 2019. Available online: https://scatterometer.knmi.nl/publications/pdf/ASCAT_Product_Manual.pdf (accessed on 4 May 2022).
42. Lin, W.; Portabella, M.; Stoffelen, A.; Vogelzang, J.; Verhoef, A. On mesoscale analysis and ASCAT ambiguity removal. *Q. J. R. Meteorol. Soc.* **2016**, *142*, 1745–1756. [CrossRef]
43. Rémy, S.; Kipling, Z.; Flemming, J.; Boucher, O.; Nabat, P.; Michou, M.; Bozzo, A.; Ades, M.; Huijnen, V.; Benedetti, A.; et al. Description and evaluation of the tropospheric aerosol scheme in the European Centre for Medium-Range Weather Forecasts (ECMWF) Integrated Forecasting System (IFS-AER, cycle 45R1). *Geosci. Model Dev.* **2019**, *12*, 4627–4659. [CrossRef]
44. Li, X.; Zhang, J.A.; Yang, X.; Pichel, W.G.; DeMaria, M.; Long, D.; Li, Z. Tropical cyclone morphology from spaceborne synthetic aperture radar. *Bull. Am. Meteorol. Soc.* **2013**, *94*, 215–230. [CrossRef]
45. Klotz, B.W.; Uhlhorn, E.W. Improved stepped frequency microwave radiometer tropical cyclone surface winds in heavy precipitation. *J. Atmos. Ocean. Technol.* **2014**, *31*, 2392–2408. [CrossRef]
46. Holbach, H.M.; Uhlhorn, E.W.; Bourassa, M.A. Off-Nadir SFMR brightness temperature measurements in high-wind conditions. *J. Atmos. Ocean. Technol.* **2018**, *35*, 1865–1879. [CrossRef]
47. Bucci, L.R.; O'handley, C.; Emmitt, G.D.; Zhang, J.A.; Ryan, K.; Atlas, R. Validation of an airborne Doppler wind lidar in tropical cyclones. *Sensors* **2018**, *18*, 4288. [CrossRef]
48. Combot, C.; Mouche, A.; Knaff, J.; Zhao, Y.; Zhao, Y.; Vinour, L.; Quilfen, Y.; Chapron, B. Extensive high-resolution synthetic aperture radar (SAR) data analysis of tropical cyclones: Comparisons with SFMR flights and best track. *Mon. Weather. Rev.* **2020**, *148*, 4545–4563. [CrossRef]
49. Zhang, G.; Li, X.; Perrie, W.; Zhang, J.A. Tropical cyclone winds and inflow angle asymmetry from SAR imagery. *Geophys. Res. Lett.* **2021**, *48*, e2021GL095699. [CrossRef]

50. Zhang, K.; Xu, X.; Han, B.; Mansaray, L.R.; Guo, Q.; Huang, J. The influence of different spatial resolutions on the retrieval accuracy of sea surface wind speed with C-2PO models using full polarization C-band SAR. *IEEE Trans. Geosci. Remote Sens.* **2017**, *55*, 5015–5025. [CrossRef]
51. Mouche, A.; Chapron, B. Global C-Band Envisat, RADARSAT-2 and Sentinel-1 SAR measurements in copolarization and cross-polarization. *J. Geophys. Res. Ocean* **2015**, *120*, 7195–7207. [CrossRef]
52. Zhang, K.; Huang, J.; Mansaray, L.R.; Guo, Q.; Wang, X. Developing a subswath-based wind speed retrieval model for Sentinel-1 VH-polarized SAR data over the ocean surface. *IEEE Trans. Geosci. Remote Sens.* **2018**, *57*, 1561–1572. [CrossRef]
53. Stoffelen, A.; Vogelzang, J. *Wind Bias Correction Guide*; EUMETSAT: Darmstadt, Germany, 2018; Volume 540.
54. Bentamy, A.; Mouche, A.; Grouazel, A.; Moujane, A.; Mohamed, A.A. Using sentinel-1A SAR wind retrievals for enhancing scatterometer and radiometer regional wind analyses. *Int. J. Remote Sens.* **2019**, *40*, 1120–1147. [CrossRef]
55. Hasager, C.B.; Hahmann, A.N.; Ahsbahs, T.; Karagali, I.; Sile, T.; Badger, M.; Mann, J. Europe's offshore winds assessed with synthetic aperture radar, ASCAT and WRF. *Wind. Energy Sci.* **2020**, *5*, 375–390. [CrossRef]
56. Gade, M.; Stoffelen, A. An introduction to microwave remote sensing of the Asian Seas. In *Remote Sensing of the Asian Seas*; Springer: Cham, Switzerland, 2019; pp. 81–101.
57. ECMWF. IFS Documentation CY47R1—Part III: Dynamics and Numerical Procedures. 2020. Available online: https://www.ecmwf.int/node/19747 (accessed on 4 May 2022).
58. Bidlot, J.-R.; Prates, F.; Ribas, R.; Mueller-Quintino, A.; Crepulja, M.; Vitart, F. Enhancing Tropical Cyclone Wind Forecasts. 2020. Available online: https://www.ecmwf.int/en/newsletter/164/meteorology/enhancing-tropical-cyclone-wind-forecasts (accessed on 4 May 2022).
59. Vogelzang, J.; Stoffelen, A. Triple collocation. In *EUTMETSAT Report*; KNMI: De Bilt, The Netherlands, 2012.
60. Lin, W.; Portabella, M.; Stoffelen, A.; Vogelzang, J.; Verhoef, A. ASCAT wind quality under high subcell wind variability conditions. *J. Geophys. Res. Ocean* **2015**, *120*, 5804–5819. [CrossRef]
61. Hoareau, N.; Portabella, M.; Lin, W.; Ballabrera-Poy, J.; Turiel, A. Error characterization of sea surface salinity products using triple collocation analysis. *IEEE Trans. Geosci. Remote Sens.* **2018**, *56*, 5160–5168. [CrossRef]
62. Vogelzang, J.; Stoffelen, A.; Verhoef, A.; Figa-Saldaña, J. On the quality of high-resolution scatterometer winds. *J. Geophys. Res. Ocean* **2011**, *116*. [CrossRef]
63. Vogelzang, J.; Stoffelen, A. Quadruple Collocation Analysis of In-Situ, Scatterometer, and NWP Winds. *J. Geophys. Res. Ocean.* **2021**, *126*, e2021JC017189. [CrossRef]
64. Vogelzang, J.; Stoffelen, A.; Lindsley, R.D.; Verhoef, A.; Verspeek, J. The ASCAT 6.25-km wind product. *IEEE J. Sel. Top. Appl. Earth Obs. Remote Sens.* **2017**, *10*, 2321–2331. [CrossRef]
65. Yang, X.; Li, X.; Pichel, W.G.; Li, Z. Comparison of ocean surface winds from ENVISAT ASAR, MetOp ASCAT scatterometer, buoy measurements, and NOGAPS model. *IEEE Trans. Geosci. Remote Sens.* **2011**, *49*, 4743–4750. [CrossRef]
66. Zhang, B.; Perrie, W. Cross-polarized Synthetic Aperture Radar: A new potential measurement technique for Hurricanes. *Bull. Am. Meteorol. Soc.* **2012**, *93*, 531–541. [CrossRef]